Unique slow dynamics and aging phenomena in soft glassy suspensions of multiarm star polymers

Brian M. Erwin,[1,2,3] Dimitris Vlassopoulos,[2,4] Mario Gauthier,[5] and Michel Cloitre[1,*]

[1]*ESPCI ParisTech, Matière Molle et Chimie (UMR ESPCI-CNRS 7167), 10 rue Vauquelin, F-75005 Paris, France*

[2]*FORTH, Institute of Electronic Structure & Laser, Heraklion GR-71110, Crete, Greece*

[3]*IBM, Hudson Valley Research Park, East Fishkill, New York 12533, USA*

[4]*University of Crete, Department of Materials Science & Technology, Heraklion GR-71300, Crete, Greece*

[5]*University of Waterloo, Department of Chemistry, Institute for Polymer Research, Waterloo, Ontario, Canada N2L 3G1*

(Received 13 March 2011; published 6 June 2011)

We use time-resolved rheology to elucidate the slow dynamics and aging in highly concentrated suspensions of multiarm star polymers. The linear and nonlinear rheological properties exhibit a terminal regime corresponding to a well-defined maximal relaxation time. Terminal relaxation is driven by arm relaxation which speeds up the escape of stars from their cages. The fact that the system fully relaxes and flows at long times has important consequences. The yield stress only exists in the limited range of frequencies or shear rates where solid-like behavior is observed. Aging is controlled by the total time elapsed after flow cessation and not by the time elapsed from flow cessation to the beginning of the measurement as in other glassy materials. Our results, which demonstrate the importance of particle architecture with respect to glassy dynamics, should be generic for long hairy particles.

DOI: 10.1103/PhysRevE.83.061402 PACS number(s): 82.70.Dd, 83.60.La, 83.60.Pq, 83.60.Rs

I. INTRODUCTION

Soft glassy materials such as foams, particulate pastes, emulsions, and micellar solutions are ubiquitous in colloidal science. In spite of their apparent diversity, these materials share several generic features that govern their dynamical properties. Their macroscopic rheology is dominated by the existence of a fluid-to-solid transition [1]. At high stresses, the materials flow very much like viscous liquids. At stresses below the so-called yield stress σ_y, they behave like solids with properties that evolve slowly with time, a phenomenon which exhibits strong similarities with the physical aging of molecular glasses and spin glasses [2]. Understanding this peculiar behavior is an outstanding challenge in statistical and condensed-matter physics, which when met could enhance our ability to design and fabricate colloidal materials for various applications and predict their long-time behavior.

The dense, amorphous structure of soft glassy materials lies at the heart of their properties. Particles are temporarily trapped in apparent cages formed by their neighbors [3]. When a stress with a magnitude greater than the yield stress is applied, they escape the cages and flow over long distances exceeding their characteristic size [4]. When the stress is removed, the crowded particles are quenched into a metastable structure, which slowly relaxes. The rheological behavior and the microscopic dynamics of out-of-equilibrium soft glassy materials below the yield stress exhibit many complex features which are not yet fully understood [5–8]. Often, these materials behave as if their longest effective relaxation time were of the order of the time they spent at rest after flow cessation. This provides a unique way to rationalize the mechanical response of aging materials in terms of the scaling variable $(t - t_w)/t_w^{\mu}$, where t is the total time after flow cessation, t_w is the time elapsed from flow cessation to the beginning of the measurement, and μ is the aging exponent [9]. This scaling works well for gels [10,11], glassy suspensions such as microgel suspensions [5,12] and colloidal suspensions [13–15], multilamellar vesicles [16], and biologically relevant materials [17]. It is nicely supported by predictions from the soft glassy rheology model [12,18]. A recent generalization of this approach using a concept of effective time corroborates the central role by the waiting time [19].

In spite of these remarkable advances, it remains unclear whether the slow dynamics of concentrated dispersions are universal. The role played by the particle microstructure is particularly challenging. While most of the soft colloids studied thus far can be viewed as simple elastic particles interacting through purely repulsive interactions, there is a dearth of research focused on the glassy and aging dynamics of soft materials with more complex architectures and/or specific interactions. In this work, we take-up this challenge for multiarm star polymers, which are representative of the wide class of hairy particles. We study model star polymers consisting of a soft corona made of f polymeric arms, each of molar mass M_a, attached to a small dendritic core [20]. The pair-interaction potential, which is purely repulsive, can be tuned from polymer-like, at low f, to hard-sphere-like, at infinite f [21]. Hence, star polymers share common features with polymers and hard-sphere colloids. In addition to being deformable [22], stars interpenetrate at high concentrations in solution, forming effective entanglements at their periphery [23–26]. In the past years, multiarm star polymers have shown utility in the study of non-hard-sphere dynamical effects in soft colloidal suspensions. In a previous report, we investigated the steady-state rheology of concentrated star solutions above the soft-jamming threshold, where they a exhibit solid-like response accompanied by yielding and flow at large stresses [27]. A recent theoretical study addresses the relationship between local packing, elasticity, and relaxation in multiarm star polymers via activated barrier hopping [28].

Here we address the slow dynamics and aging that takes place when star solutions are subjected to stresses lower than

*michel.cloitre@espci.fr

the yield stress. We show that soft jammed star solutions exhibit unique history-dependent phenomena that are not observed in other colloidal or polymeric glasses. Rheological aging proceeds in three different regimes: a short-time interval immediately after rejuvenation, a nonstationary regime at intermediate times where the properties evolve slowly, and a long-time regime where, surprisingly, star glasses ultimately reach mechanical equilibrium. The viscoelastic moduli and the stress vary with the angular frequency and the shear rate, respectively, where they each exhibit a terminal low-frequency (or low-rate) regime corresponding to a well-defined maximal relaxation time. Because of this, the strain response to a mechanical stress scales with the total time t elapsed after rejuvenation instead of the waiting time t_w as is usually the case for particulate suspensions. We discuss our results in light of the structure and the dynamics of star polymers. These experiments offer direct evidence that aging in soft colloidal systems is not universal and can be influenced by specific microscopic mechanisms.

The paper is organized as follows: Sec. II describes the materials and the rheological procedures used to characterize the aging behavior of the suspensions. In Sec. III, we analyze the linear and nonlinear behavior of star suspensions using time-resolved rheology, we discuss the role of concentration, and we characterize aging and slow dynamics. The results are discussed in Sec. IV, and the key conclusions are summarized in a final section.

II. EXPERIMENTS

A. Materials

We used 1,4-polybutadiene stars with a weight-average branching functionality of 390 arms, each having a weight-average molar mass of 24.4 kg/mol. The anionic synthesis and the characterization of these stars have been described in detail previously [20,29,30]. We prepared solutions of stars in squalene, which is a good solvent for polybutadiene, by using the established methodology for complete dissolution [25]. Tetrahydrofuran (THF) was added in excess as a cosolvent in order to facilitate the dispersion and mixing of the stars in squalene. THF was then evaporated under continuous mixing and a vacuum was applied as a finishing step to ensure full removal of the cosolvent. In dilute solutions, the stars have a nearly spherical shape with a hydrodynamic radius $R_h = 40$ nm at 20 °C. The overlap concentration $C^* = 3fM_a/(4\pi N_A R_h^3)$ was estimated at 57 mg/ml (N_A is Avogadro's number). For $C>100$ mg/ml, the solutions exhibit all the hallmarks of glassy behavior: (i) a plateau modulus higher than the loss modulus exists over an extended range of frequencies; (ii) a yield stress σ_y which can be characterized using oscillatory strain sweep measurements; (iii) slow dynamics are present; and (iv) aging takes place. The data we report have been obtained for two concentrations in the glassy regime; namely, $C = 109$ and 150 mg/ml, for which $\sigma_y = 27$ and 150 Pa, respectively [27].

B. Rheology

The slow dynamics of the solutions were studied by stress- and strain-controlled rheology. We used an Anton-Paar MCR501 rheometer mounted with a cone and Peltier plate geometry with a diameter of 25 mm, a 2° angle, and a truncation of 48 μm. The shearing surfaces were coated with chromium to provide a surface roughness of 2–4 μm which, in combination with the good affinity of the stars with metallic surfaces, prevents slip [25]. All measurements were made at a temperature of 20.0 ± 0.1 °C using the following protocol: (i) a preshearing stress larger than the yield stress σ_y was applied for a time $t_p \geqslant 30$ s; (ii) at $t = 0$, the stress was set to zero and the sample was allowed to relax for a time t_w; (iii) the rheological tests started at $t_w \geqslant 0$. Preshearing fully fluidizes the solution and brings it to a reproducible nonequilibrium state [5,25]. Its duration was sufficiently long for t_p to play no role in the results presented below. We performed three types of tests: oscillatory time sweep experiments where the storage modulus G' and loss modulus G'' were measured as a function of time t and angular frequency ω and at a fixed strain amplitude γ_0; constant shear rate experiments where the stress was measured as a function of time and applied shear rate; and creep experiments where the strain and the shear rate were measured as a function of time and applied stress. These data were analyzed to provide snapshots of the time-dependent shear stress and viscoelastic moduli at predefined times [31]. The frequency dependence of the viscoelastic moduli at fixed sample age t was reconstructed from a series of oscillatory time-sweep data across different frequencies. Similarly, time-resolved flow curves were obtained from the transient-shear and creep data. This procedure allows for the extraction of the frequency and time-dependent storage $G'(\omega, t)$, loss $G''(\omega, t)$, and complex modulus $G^*(\omega, t)$, as well as the time-dependent flow curves, $\sigma(\dot{\gamma}, t)$.

III. RESULTS

A. Time-resolved rheology of star solutions

We performed oscillatory time sweeps with small strain amplitudes to measure the time-dependent linear viscoelastic properties of star solutions. Figure 1 shows how the storage and loss moduli of a solution at $C = 109$ mg/ml evolve as a function of time for different applied angular frequencies ω. At high frequencies both moduli appear independent of time, while at low frequencies they vary with time. For frequencies $\omega = 3.2$–0.32 rad/s, where $G'(\omega, t)$ is larger than $G''(\omega, t)$, $G'(\omega, t)$ increases slowly as $G''(\omega, t)$ decreases. For $\omega < 0.32$ rad/s, where both moduli increase with time, the loss modulus is larger than the storage modulus, suggesting that the viscoelastic properties of the solution are approaching terminal behavior at low frequencies.

Constant shear rate experiments and creep experiments were used to explore the time-dependent nonlinear rheology of the star solutions. Figure 2 shows shear data collected from a series of experiments where fixed shear rates $\dot{\gamma}$, spanning seven orders of magnitude, were applied at $t = 0$. At the largest applied shear rate, the stress reaches a time-independent plateau that is larger than the yield stress value σ_y, obtained from oscillatory strain sweeps. At each of the lesser shear rates, the stress first evolves during about 4×10^4 s before reaching a constant value smaller then σ_y. This shows that the material ultimately reaches steady state at very long times. In practice

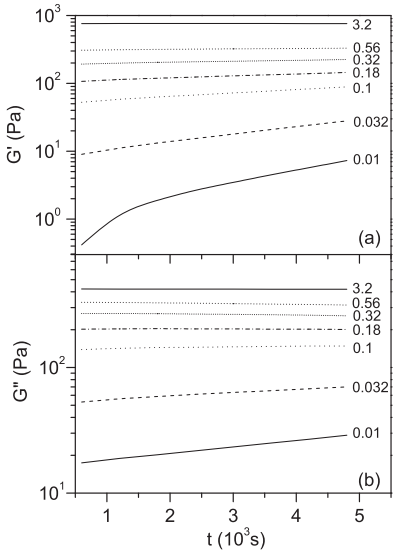

FIG. 1. Storage (a) and loss moduli (b) as a function of time for $\gamma_0 = 1\%$ and different applied angular frequencies. From bottom to top, $\omega = 0.01$, 0.032, 0.1, 0.18, 0.32, 0.56, and 3.2 rad/s.

we note that the manner and the time required to reach the steady state can depend on the applied shear rate.

Figure 3 shows the results of creep measurements for a range of applied stresses spanning two orders of magnitude, each applied at $t = 0$. For stresses much larger than the yield stress σ_y, the shear rate reaches a constant value a few seconds after the application of the stress. For stresses near to and lower than σ_y, the shear stress evolves over about 4×10^4 s before reaching the steady state. As was noted for constant shear rate experiments, the time required to reach steady state depends on the applied rate. Again, the interesting result here is that the solution ultimately reaches the steady state.

B. Role of concentration

To explore the generality of the results described in the previous section, we have performed long-term creep experiments on star solutions prepared at different concentrations. For the sake of comparison, we report here data for stresses approximately equal to a constant fraction of the respective

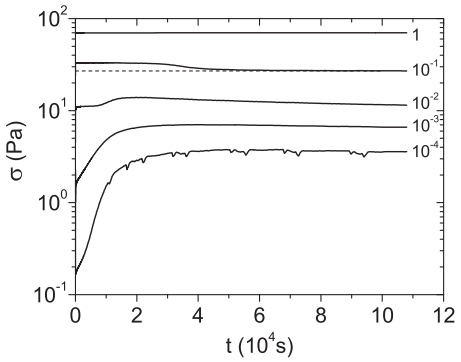

FIG. 2. Shear stress as a function of time and applied shear rate. From bottom to top, $\dot{\gamma} = 10^{-4}$, 10^{-3}, 10^{-2}, 10^{-1}, and 1 s^{-1}. The dashed line indicates the yield stress from oscillatory strain sweeps ($\sigma_y = 27$ Pa).

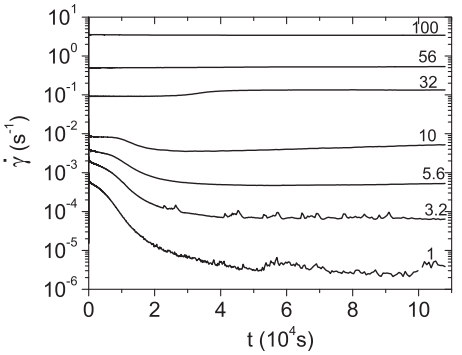

FIG. 3. Shear rate as a function of time for creep experiments. From bottom to top, $\sigma = 1$, 3.2, 5.6, 10, 32, 56, and 100 Pa.

yield stress for each solution ($\sigma \approx 0.15\sigma_y$). They are plotted in Fig. 4 using a double logarithmic scale. Each experiment exhibits the same qualitative behavior. The application of the stress is followed by a transient response which lasts for about 50 s. The shear rate then reaches an intermediate-time regime where it decreases steadily. At long times, the shear rate ultimately reaches a constant value indicating that the samples have reached or are approaching the steady-state. Although the curves in Fig. 4 all show similar trends, we note some interesting differences. The decrease of the shear rate in the intermediate regime is steeper, the drop before the long-time regime is less pronounced, and the latter shows up later when the concentration is higher. For $C = 150$ mg/ml, the shear rate keeps on evolving, albeit very slowly, at time scales as long as 10^5 s. Much longer experiments with better torque resolution would be required to establish whether the solution has definitely reached the steady state. However, this does not affect our main message. Below the yield stress, the rheological properties display unusual aging behavior before equilibrating at very long times.

C. Aging of star solutions

We then investigated the aging properties of star solutions by varying the mechanical history. Figure 5(a) depicts the time evolution of the strain measured via long-term creep

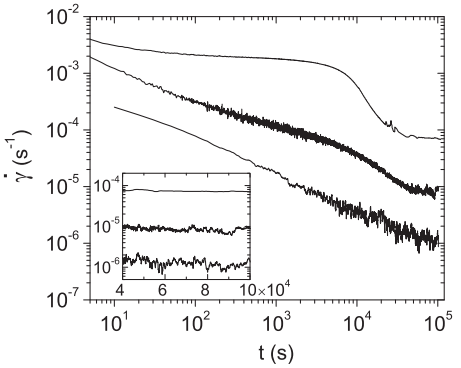

FIG. 4. Shear rate variations from creep experiments ($t_w = 0$) in star solutions at $C = 109$, 125, and 150 mg/ml and $\sigma = 3.8$, 10, and 30 Pa, respectively (from top to bottom). The inset shows the long-time variations ($t \geqslant 4 \times 10^4$ s) using linear coordinates for the time axis.

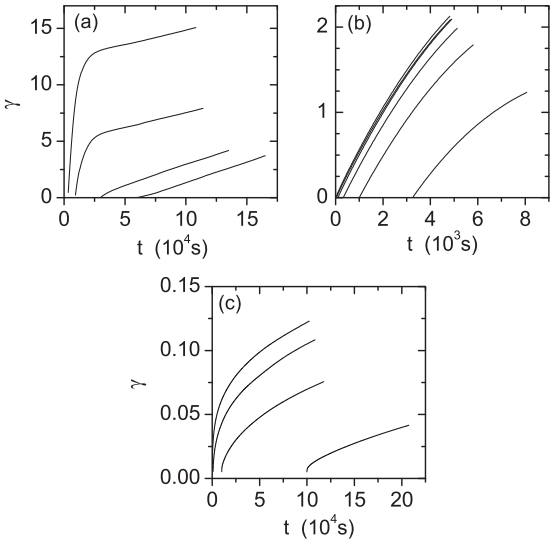

FIG. 5. Graphs (a) and (b) show creep data for the 109 mg/ml solution with $\sigma = 1$ Pa and different waiting times t_w; (a) long-term strain variations for $t_w = 3\times10^3$, 9×10^3, 3×10^4, and 6×10^4 s (from left to right); (b) strain variations at intermediate times for $t_w = 10$, 32.6, 100, 326, 100, and 3260 s (from left to right). Graph (c) shows creep data for the 150 mg/ml solution with $\sigma = 20$ Pa; from left to right: $t_w = 10$, 10^2, 10^3, and 10^4 s.

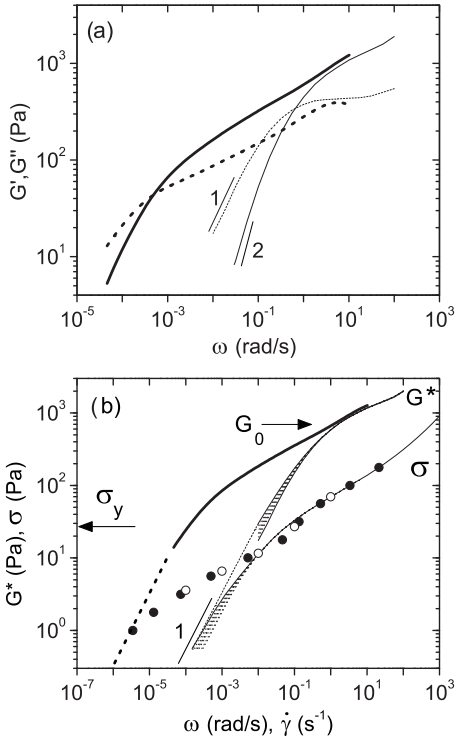

FIG. 6. (a) Storage (—) and loss (- - - -) moduli as function of angular frequency for the $C = 109$ mg/ml solution at $t = 600$ s (thin lines) and $t = 6\times10^4$ s (thick lines). (b) Complex modulus and shear stress as functions of angular frequency and shear rate, respectively. Dotted curves refer to G^* and σ data sampled at $\Delta t = 600$ s intervals and collected up to $t = 4800$ s (thin solid curves). The thick solid curve (G^*) and the symbols (○, ●: flow curve data from controlled stress and controlled strain experiments, respectively) refer to equilibrated samples at $t = 6 \times 10^4$ s. The dashed straight lines in (b) are extrapolations of the complex moduli measured at $t = 4800$ s and $t = 6 \times 10^4$ s to low frequencies.

experiments for $C = 109$ mg/ml, when the waiting time t_w elapsed from the end of preshear to the stress application was varied from 0 to 6×10^4 s. Clearly, the value of $\gamma(t)$ at a given time t depends on t_w. At long times, the different creep curves increase linearly with time; they have the same slope, indicating that the steady-state shear rate is independent of t_w. The time regime preceding the steady state is studied in more detail in Fig. 5(b), which presents the variation in $\gamma(t)$ for a range of waiting times between 10 and 3260 s. We observe that creep is lower when the waiting time is longer. Figure 5(c) shows the results of similar creep experiments performed on a solution at $C = 150$ mg/ml. The different creep curves exhibit the same qualitative behavior as in Figs. 5(a) and 5(b), supporting the generality of the results presented.

IV. DISCUSSION

A. State diagram

Figure 6(a) presents the time-dependent viscoelastic moduli for the $C = 109$ mg/ml solution at intermediate and long times. The data for $t = 600$ s were obtained from multiple oscillatory time sweeps at variable frequencies as explained in Sec II B. The moduli for $t = 6 \times 10^4$ s (i.e., at a time when the solution had reached steady state) were determined from the linear stress relaxation function [25]. Both sets of data exhibit the same characteristic features. At intermediate frequencies, the storage modulus depends weakly on frequency and exceeds the loss modulus, indicating elastic behavior. At low frequencies, the loss modulus becomes larger than the storage modulus and both decrease with decreasing frequency as power laws, indicating viscoelastic relaxation. The onset of the low-frequency region, which is associated with the inverse of the longest relaxation time of the material, shifts to lower frequencies by about three decades as the solution ages. Terminal relaxation is unambiguously observed at $t = 600$ s but barely at $t = 6 \times 10^4$ s, for which reliable data at very low frequencies could not be obtained.

In Fig. 6(b), we analyze the evolution of the linear and nonlinear rheological properties during aging by plotting the time-dependent complex moduli and shear stresses at different times t versus frequency and shear rate, respectively. The series of complex moduli data $G^*(\omega,t) = [G'^2(\omega,t) + G''^2(\omega,t)]^{1/2}$ were obtained from multiple oscillatory time sweeps using a sampling time $\Delta t = 600$ s; the long-time modulus at $t = 6 \times 10^4$ s was calculated from the storage and loss moduli shown in Fig. 6(a). The series of flow curves $\sigma(\dot\gamma,t)$ were constructed from the variations of $\dot\gamma(t)$ and $\sigma(t)$ measured in constant shear rate and creep experiments, respectively, also sampled at $\Delta t = 600$ s. This comparison reveals several interesting features of the microscopic dynamics associated with aging. At intermediate frequencies and shear rates, $\sigma(\dot\gamma,t)$ is much smaller than $G^*(\omega,t)$, indicating that the equilibrium structure is disrupted and that the solution is fully rejuvenated. The stress slowly decreases with decreasing shear rate. Moreover, at and below the yield stress σ_y measured from oscillatory strain sweep experiments, the stress keeps on decreasing with

decreasing shear-rate as a power-law with a weak exponent. Thus, in these star solutions, the yield stress is nothing like a yield stress defined as the low shear rate plateau of the flow curve. At low frequencies and shear rates, the trajectories describing $G^*(\omega,t)$ and $\sigma(\dot{\gamma},t)$ are proportional to ω and $\dot{\gamma}$, respectively. The extrapolations of the $G^*(\omega,t)$ curves to very low frequencies coincide with the low shear-rate portions of the flow curves. These observations altogether confirm that the linear and nonlinear rheological properties of star solutions at low frequencies or shear rates are driven by the same relaxation process which ultimately leads to terminal behavior. Aging manifests itself by a shift of the terminal regime towards lower frequencies (or shear rates), which does not significantly affect the value of the elastic plateau at high frequencies ($\omega > 1$ rad/s) or the weak power-law plateau of the flow curve. Finally, we note that the data obtained from controlled-strain and controlled-stress experiments fall on the same flow curve, which a priori rules out the possibility of shear-banded flow as has been observed in other star polymer solutions [31].

B. Origin of terminal relaxation in star solutions

The above results can be rationalized by revisiting the conventional cage picture used to describe the dynamics of colloidal glasses. Within this framework, each particle is constrained in a cage formed by a small number of neighbors, which restrict and eventually arrest macroscopic motion. At very short times, particles move locally within the cages via a process called β-relaxation. At much longer times, particles eventually escape from their cages via a thermally-activated process termed the α-relaxation, which represents the longest relaxation of the material. This process marks the glass-to-fluid transition. This picture has proven extremely successful in describing the dynamics of hard-sphere glasses [3,32,33]. The β-relaxation, which is due to the fast rattling motion of particles inside their cage, takes place at frequencies generally not accessible by conventional rheology. The α-relaxation is associated with the existence of a nontrivial, exponential divergence of the characteristic time τ_α at a critical volume fraction close to that of the jamming transition [33].

The cage picture should apply to star solutions with some important modifications. First, the interaction potential, although purely repulsive, is much softer than in hard-sphere suspensions [21]. Secondly, at contact, stars partly interpenetrate by forming effective entanglements between the outer blobs [23], as revealed by dynamic light scattering investigations of cooperative diffusion [26]. With these peculiarities in mind, we can now combine the polymeric nature of star polymers and the cage concept to build the following microscopic picture. At rest, stars are jammed and the macroscopic motion between neighboring stars is drastically hindered, so that the rheological response is dominated by elasticity associated with caging and arm interpenetration. The application of a large stress breaks the cages and induces rearrangements, causing shear thinning. This picture is qualitatively supported by the nearly-plateau modulus of $G^*(\omega,t)$ at higher frequencies and by the existence of a yield stress. At long time, terminal relaxation must proceed through both cage escape like in hard-sphere glasses and the disengagement of stars from their neighbors [25]. In practice, arm relaxation causes the deformation of the coronas, speeds-up terminal motion via fluctuations, and facilitates long-time relaxation [34]. This thermally-activated process drives the long-time relaxation of the linear and nonlinear rheological properties, making it observable over experimentally accessible frequencies and shear rates. A direct consequence of this is that the yield stress exists over the limited range of frequencies above the inverse of the terminal relaxation time. When shearing at the lowest shear rates, the mechanical energy put into the system is dissipated and does not contribute to colloidal rearrangements. This bears analogy to the so-called elastic yielding phenomenon of highly entangled polymer solutions [35]. As the material ages, terminal relaxation becomes slower and slower but remains accessible, albeit at very long times. Of course, as the volume fraction of the stars is increased, relaxation takes longer to appear and the terminal time shifts to lower frequencies and shear rates, but the physics remains essentially unchanged, as shown in Fig. 4.

C. Unique aging properties of star solutions

The presence of an accessible long-time relaxation process in star solutions explains the aging properties presented in Sec. III B. Indeed, according to conventional viscoelasticity theory, the mechanical stress can be expressed as $\sigma(t) = \int_0^t G\left(t-t',t'\right)\dot{\gamma}\left(t'\right)dt'$. Since the stress relaxation function decays more rapidly than the time over which the solutions age, we can approximate $\dot{\gamma}(t')$ by $\dot{\gamma}(t)$ and we obtain $\sigma(t) = \dot{\gamma}(t)\int_0^t G\left(t-t',t'\right)dt'$. Thus, the long-time rheological properties must be functions of the total time elapsed after the end of rejuvenation only. This result is a direct physical consequence of the fact that the dynamics in the terminal regime are essentially driven by a detectable, thermally activated cage-escape process.

The application of any small stress during the waiting time $t_w < \tau_\alpha$ does not affect the state of the material, since the energy brought to the system is dissipated without contributing to colloidal rearrangements. Figures 7(a) and 7(b), obtained for $C = 109$ and $C = 150$ mg/ml, respectively, show that the variations in the shear rate for different waiting times t_w do form a master curve that depends only on the total time elapsed after the end of preshear. A straightforward consequence is that the strain responses obtained for different t_w must be identical to within additive factors γ_m, which correspond to the strains accumulated between preshear cessation ($t = 0$) and the stress application ($t = t_w$): $\gamma_m(t_w) = \int_0^{t_w}\dot{\gamma}\left(t'\right)dt'$. This result is well confirmed by the data shown in Figs. 7(c) and 7(d). The analytical form of $\gamma_m(t_w)$ is directly related to the variations in $\dot{\gamma}(t)$, as shown in Figs. 7(e) and 7(f). For $C = 109$ mg/ml, the shear rate decreases linearly with time according to $\dot{\gamma}(t) = \dot{\gamma}_0(1 - t/t_\infty)$ where $\dot{\gamma}_0 = 5.9 \times 10^{-4}$ s and $t_\infty = 10^4$ s. Thus the strain factor corresponds to the expression $\gamma_m(t_w) = \dot{\gamma}_0 t_w(1 - t_w/2t_\infty)$, in agreement with the data plotted in Fig. 7(e). For $C = 150$ mg/ml, the time dependence of the shear rate follows a power law $\dot{\gamma}(t) \propto t^{-0.66}$, from which we deduce that $\gamma_m(t_w) \propto t_w^{0.34}$ as found in Fig. 7(f). It is interesting to note that the data for $C = 150$ mg/ml are reminiscent of the Andrade creep behavior which is observed in many plastically deforming crystalline and amorphous materials [36,37]. More experiments would be required to establish the generality of this result.

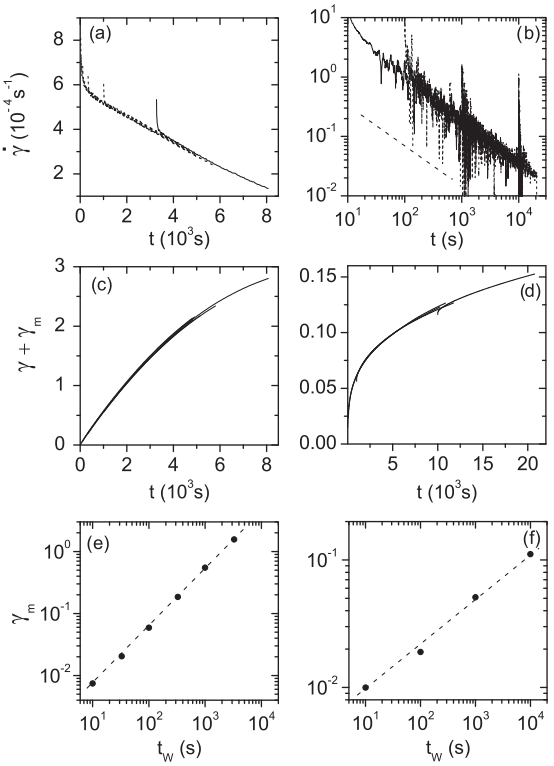

FIG. 7. (a) Apparent shear rates from Fig. 5(b) for $C = 109$ mg/ml against total time after flow cessation (from left to right: $t_w = 10$, 32.6, 100, 326, 100, and 3260 s). (b) Apparent shear rates from Fig. 5(c) for $C = 150$ mg/ml in double logarithmic coordinates (from left to right: $t_w = 10$, 10^2, 10^3, and 10^4 s); the dashed line has a slope 0.66. (c) Reduced strain curve obtained by shifting vertically the data shown in Fig. 5(b) for $C = 109$ mg/ml. (d) Reduced strain curve obtained by shifting vertically the data shown in Fig. 5(c) for $C = 150$ mg/ml. (e), (f) Variation of the shift parameters γ_m used to obtain the master curves (c) and (d) against waiting time; the dashed lines have slopes 1 and 0.34, respectively.

V. Concluding remarks

Summarizing our results, the aging properties of the arrested suspensions of star polymers studied here are characterized by the following unique properties: (i) aging proceeds in successive regimes before reaching steady state; (ii) terminal relaxation is reached at low frequencies and shear rates; (iii) aging is associated with a slowing-down of terminal relaxation at low frequencies and shear rates; (iv) at intermediate times, nonlinear creep data depend on the total time elapsed after rejuvenation and not on the waiting time.

Successive aging regimes have been observed in some systems but with very different characteristics. In colloidal gels [10] and laponite suspensions [15], aging proceeds through an initial process where the relaxation time of the dynamic structure factor is an exponential function of t_w and a long-time process, termed "full aging," where it increases linearly with t_w. In hard-sphere glasses the relaxation time shows full aging behavior at early times and ultimately reaches equilibrium at long times [38,39]. It is also noteworthy, however, that the waiting time always plays a central role in these materials, in contrast with the case of star solutions.

Similarly, the rheological properties of jammed colloidal materials generally do not exhibit the unique combination of aging and terminal relaxation observed in this work. In most materials, such as emulsions, colloidal suspensions and multilamellar vesicles, individual particles are trapped into metastable environments from which they do not escape over accessible time scales. To put it simply, their α-relaxation is too long or even does not exist. Consequently, the storage modulus and the shear stress usually remain nearly constant down to the lowest accessible frequencies and shear rates, where additional phenomena such as shear banding eventually come into play [40,41].

The existence of a well-defined maximal relaxation time, which is short compared to the timescale on which it evolves, explains the scaling of the creep data with the total time elapsed after flow cessation. This property also distinguishes star suspensions from other soft glassy materials where the rheological quantities measured by creep and stress relaxation are rationalized in terms of simple functions of t/t_w.

All these observations suggest that arrested suspensions of star polymers belong to a new class of soft glassy materials. Our results, which demonstrate the importance of particle architecture with respect to glassy dynamics, should be generic for long hairy particles. An interesting question, however, is how functionality and arm length influence the details of the phenomena reported in this work. From a previous study, we already have strong indications that α-relaxation driven by arm disengagement is found in other star suspensions, albeit with some complications associated with shear banding [31,42,43]. This question prompts us to further investigations where the star architecture will be systematically and rationally varied.

ACKNOWLEDGMENTS

B.E. acknowledges financial support from EU NoE Soft-Comp, Grant No. NMP3-CT-2004-502235. This work was performed in part when D.V. was visiting the Soft Matter and Chemistry laboratory at ESPCI ParisTech with the support of the "Michelin Chair at ESPCI ParisTech". M.G. thanks the Natural Sciences and Engineering Research Council of Canada (NSERC) for financial support.

[1] H. A. Barnes, J. Non-Newtonian Fluid Mech. **81**, 133 (1999).

[2] *Slow Relaxations and Nonequilibrium Dynamics in Condensed Matter*, edited by J.-L. Barrat, M.V. Feigelman, J. Kurchan, and J. Dalibard (Springer, Berlin, 2003).

[3] P. N. Pusey, in *Liquids, Freezing and Glass Transition*, edited by J. P. Hansen, D. Levesque, and J. Zinn-Justin (Elsevier, Amsterdam, 1991).

[4] M. Fuchs and M. E. Cates, Phys. Rev. Lett. **89**, 248304 (2002).

[5] M. Cloitre, R. Borrega, and L. Leibler, Phys. Rev. Lett. **85**, 4819 (2000).
[6] F. Da Cruz, F. Chevoir, Daniel Bonn, and P. Coussot, Phys. Rev. E **66**, 051305 (2002).
[7] V. Viasnoff and F. Lequeux, Phys. Rev. Lett. **89**, 065701 (2002).
[8] A. Negi and C. Osuji, Europhys. Lett. **90**, 28003 (2010).
[9] L. C. E. Struik, *Physical Aging in Amorphous Polymers and Other Materials* (Elsevier, Amsterdam, 1978).
[10] L. Cipelletti, S. Manley, R. C. Ball, and D. A. Weitz, Phys. Rev. Lett. **84**, 2275 (2000).
[11] B. Chung, S. Ramakrishnan, R. Bandyopadhyay, D. Liang, C. F. Zukoski, J. L. Harden, and R. L. Leheny, Phys. Rev. Lett. **96**, 228301 (2006).
[12] E. H. Purnomo, D. van den Ende, S. A. Vanapalli, and F. Mugele, Phys. Rev. Lett. **101**, 238301 (2008).
[13] C. Derec, A. Ajdari, G. Ducouret, and F. Lequeux, C. R. Acad. Sci. Paris Ser. IV **1**, 1115 (2000).
[14] B. Abou, D. Bonn, and J. Meunier, Phys. Rev. E **64**, 021510 (2001).
[15] M. Bellour, A. Knaebel, J. L. Harden, F. Lequeux, and J.-P. Munch, Phys. Rev. E **97**, 031405 (2003).
[16] L. Ramos and L. Cipelletti, Phys. Rev. Lett. **87**, 245503 (2001).
[17] P. Bursac, G. Lenormand, B. Fabry, M. Oliver, D. A. Weitz, V. Viasnoff, and J. P. Butler, Nat. Mater. **4**, 557 (2005).
[18] S. M. Fielding, P. Sollich, and M. E. Cates, J. Rheol. **44**, 323 (2000).
[19] A. Shahin and Y. M. Joshi, Phys. Rev. Lett. **106**, 038302 (2011).
[20] J. Roovers, L. L. Zhou, P. M. Toporowski, M. van der Zwan, H. Iatrou, and N. Hadjichristidis, Macromolecules **26**, 4324 (1993).
[21] C. N. Likos, H. Löwen, M. Watzlawek, B. Abbas, O. Jucknischke, J. Allgaier, and D. Richter, Phys. Rev. Lett. **80**, 4450 (1998).
[22] E. Stiakakis, G. Petekidis, D. Vlassopoulos, C. N. Likos, H. Iatrou, N. Hadjichristidis, and J. Roovers, Europhys. Lett. **72**, 664 (2005).
[23] M. Daoud and J. P. Cotton, J. Phys. (Paris) **43**, 531 (1982).
[24] C. N. Likos, Phys. Rep. **348**, 267 (2001).
[25] M. Helgeson, N. J. Wagner, and D. Vlassopoulos, J. Rheol. **51**, 297 (2007).
[26] A. N. Semenov, D. Vlassopoulos, G. Fytas, G. Vlachos, G. Fleischer, and J. Roovers, Langmuir **15**, 358 (1999).
[27] B. M. Erwin, M. Cloitre, M. Gauthier, and D. Vlassopoulos, Soft Matter **6**, 2825 (2010).
[28] J. Yang and K. S. Schweizer, Eur. Phys. Lett. **90**, 66001 (2010).
[29] J. Roovers, P. Toporowski, and J. Martin, Macromolecules **22**, 1897 (1989).
[30] M. Gauthier and A. Munam, Macromolecules **43**, 3672 (2010).
[31] B. E. Erwin, D. Vlassopoulos, and M. Cloitre, J. Rheol. **54**, 915 (2010).
[32] P. N. Pusey and W. van Megen, Phys. Rev. Lett. **59**, 2083 (1987).
[33] G. Brambilla, D. El Masri, M. Pierno, L. Berthier, L. Cipelletti, G. Petekidis, and A. B. Schofield, Phys. Rev. Lett. **102**, 085703 (2009).
[34] M. Kapnistos, A. N. Semenov, D. Vlassopoulos, and J. Roovers, J. Chem. Phys. **111**, 1753 (1999).
[35] C. P. Boukany and S. Q. Wang, Macromolecules **42**, 2222 (2009).
[36] M.-C. Miguel, A. Vespignani, M. Zaiser, and S. Zapperi, Phys. Rev. Lett. **89**, 165501 (2002).
[37] M.-C. Miguel, J. S. Andrade Jr., and S. Zapperi, Braz. J. Phys. **33**, 557 (2003).
[38] D. El Masri, M. Pierno, L. Berthier, and L. Cipelletti, J. Phys. Condens. Matter **17**, S3543 (2005).
[39] V. A. Martinez, G. Bryant, and W. van Megen, Phys. Rev. Lett. **101**, 135702 (2008).
[40] S. M. Fielding, M. E. Cates, and P. Sollich, Soft Matter **5**, 2378 (2009).
[41] P. Coussot and G. Ovarlez, Eur. Phys. J. E **33**, 183 (2010).
[42] R. L. Moorcroft, M. E. Cates, and S. M. Fielding, Phys. Rev. Lett. **106**, 055502 (2011).
[43] C. Christopoulou, G. Petekidis, B. E. Erwin, M. Cloitre, and D. Vlassopoulos, Philos. Trans. R. Soc. London A **367**, 5051 (2009).